Chemical Science

ROYAL SOCIETY OF CHEMISTRY

EDGE ARTICLE

View Article Online
View Journal | View Issue

Cite this: *Chem. Sci.*, 2022, **13**, 12114

All publication charges for this article have been paid for by the Royal Society of Chemistry

Received 15th July 2022
Accepted 15th September 2022

DOI: 10.1039/d2sc03947h

rsc.li/chemical-science

Surface enrichment of Ir on the IrRu alloy for efficient and stable water oxidation catalysis in acid†

Junming Zhang, ‡[a] Xueli Cao,‡[b] Ya-Fei Jiang, ‡[c] Sung-Fu Hung, [d] Wei Liu, [e] Hong Bin Yang,[e] Cong-Qiao Xu, [c] Dong-Sheng Li, [f] Tianyu Zhang,*[g] Yujing Li, *[h] Jun Li[ci] and Bin Liu *[a]

Inducing the surface enrichment of active noble metal can not only help to stabilize the catalyst but also modify the catalytic performance of the catalyst through electronic and geometric effects. Herein, we report the *in situ* surface enrichment of Ir on IrRu alloy during the oxygen evolution reaction (OER). The surface enrichment of Ir was probed by *ex situ* high-resolution transmission electron microscopy (HRTEM), *in situ* X-ray absorption spectroscopy (XAS), and electrochemical Cu stripping, leading to complementary characterizations of the dynamic reconstruction of the IrRu alloy during OER. Guided by the density functional theory (DFT), an IrRu alloy with low Ir content (20 wt%) was constructed, which displayed a low overpotential of only 230 mV to deliver an OER current density of 10 mA cm^{-2} in 0.1 M $HClO_4$ solution and maintained stable performance for over 20 h. To investigate the practical application potential, a proton exchange membrane (PEM) water electrolyzer using the IrRu alloy as the anode catalyst was assembled, which required a low cell voltage of only 1.48 V to generate a current density of 1 A cm^{-2}.

Introduction

Hydrogen is considered as the ultimate energy carrier as obtaining energy by oxidizing hydrogen produces only water, which greatly pushes the goal towards carbon neutrality. To promote the environment-friendly production of hydrogen, water electrolysis powered by renewable electricity stands out as a promising route, including proton exchange membrane (PEM) water electrolyzer, alkaline exchange membrane (AEM) water electrolyzer, and solid oxide electrolyzer (SOE). Among them, PEM water electrolyzer has the advantages of much higher current and power density, lower resistance, thinner membrane, lower gas crossover, shorter start-up times, and wider operating temperatures with smaller stack areas, which contribute to the development of water electrolyzer stacks with lower costs.[1] However, the performance of PEM water electrolyzer is still severely limited by its anode, where the catalyst sustains high oxidation potential as well as a strong acidic environment.[2] Currently, noble metals, especially Ru and Ir, are the only choices that give acceptable performance for the acidic oxygen evolution reaction (OER). Ru is the most active element for acidic OER; however, it is very unstable due to the dissolution of high valence ruthenium oxides under oxidative potentials.[3] Zhao *et al.* reported defect-rich RuO_2 nanosheets, which could reduce the acidic OER overpotential at 10 mA cm^{-2} to 210 mV but only sustained no more than 6 h.[4] By co-alloying Ru with other transition metals (*e.g.*, Cr[5] and Co[6]), its stability could be improved but still it is far from being acceptable. In comparison, Ir is much more stable in acidic OER.[7] However, its activity is inferior to Ru and it is also more expensive than Ru.

To maintain an optimal balance between performance and cost, minimizing the noble metal usage and at the same time making full use of every noble metal site is an effective

[a]*School of Chemical and Biomedical Engineering, Nanyang Technological University, Singapore 637459, Singapore. E-mail: liubin@ntu.edu.sg*

[b]*Department of Chemistry, Zhejiang University, Hangzhou 310027, China*

[c]*Department of Chemistry, Southern University of Science and Technology, Shenzhen 518055, China*

[d]*Department of Applied Chemistry, National Yang Ming Chiao Tung University, Hsinchu 300, Taiwan*

[e]*Dalian Institute of Chemical Physics, Chinese Academy of Sciences, Dalian 116023, China*

[f]*College of Materials and Chemical Engineering, Key Laboratory of Inorganic Nonmetallic Crystalline and Energy Conversion Materials, China Three Gorges University, Yichang 443002, China*

[g]*College of Environmental Science and Engineering, Beijing Forestry University, Beijing 100083, China. E-mail: tzhang@bjfu.edu.cn*

[h]*School of Materials Science and Engineering, Beijing Institute of Technology, Beijing 100081, China. E-mail: yjli@bit.edu.cn*

[i]*Department of Chemistry and Key Laboratory of Organic Optoelectronics and Molecular Engineering of Ministry of Education, Tsinghua University, Beijing 100084, China*

† Electronic supplementary information (ESI) available: Materials and methods, Fig. S1–S9, Tables S1–S6 (PDF). See https://doi.org/10.1039/d2sc03947h

‡ These authors contributed equally to this work.

strategy.[4,8–10] Loading active metal on the support can increase the active metal dispersity; however, it is only applicable to a few acid-resistant supports, considering the harsh reaction environment.[11–16] Besides, tuning the intrinsic performance of OER catalysts is crucial. This can be achieved by alloying Ir or Ru with noble and/or non-noble metals, by which the electronic structure can be tuned with high flexibility. Selected examples include IrAu,[17] IrW,[18] IrSr,[19,20] IrLi,[21] IrNi,[2,22–24] RuCr,[5] and RuY.[6,25–28] Among these, the IrRu alloy exhibits the highest acidic OER performance by maximizing the merits of both metals.[6,13,18,26,27,29–43] Although extensive efforts have been devoted to developing IrRu alloy OER electrocatalysts, few can achieve both high catalytic activity and stability at a low Ir content (*i.e.*, Ir < 20 wt%).[4]

To further balance cost and stability, structures with Ir oxide surface and heterogeneous core were designed and constructed by simple deposition,[32] chemical leaching,[24] electrochemical leaching,[2,19,20,23,38,44] annealing induced surface segregation,[42,43] and sequential reduction.[33] The core could tune the surface electronic structure for better reactivity, while the Ir-only surface could maintain structural stability due to its much higher acid endurance.[32,33,37] However, the poor tunability of the shell could cause troubles. If the Ir enriched shell is too thick, the core could hardly influence the electronic structure of the shell, and the intrinsic activity will not be optimized, not to mention the increased high cost induced by the thick Ir shell.[33] If the shell is too thin or porous, the shell will not be able to protect the core from dissolution. Hence, a promising structure can be expected as the Ir-rich shell with proper thickness can balance the protection to the core from the reactive reaction and at the same time maintain an effective electronic interaction triggered by the core.

Herein, we reported an IrRu alloy catalyst loaded on TiC that could *in situ* form an Ir-enriched surface during OER. This Ir-enriched surface could protect Ru from dissolution in the core, and the adsorption energetics of the Ir shell to OER intermediates could be tuned by varying the Ir/Ru ratio. The precise surface structure was probed by both microscopic and electrochemical characterizations, and *operando* X-ray absorption spectroscopy (XAS) detected the valence state and coordination environment change during the reaction, verifying the *in situ* surface reconstruction to form the Ir-enriched shell, which greatly improved the catalytic stability in acidic OER. The IrRu alloy (Ir/Ru = 1/4) on TiC exhibited an overpotential as low as 230 mV at 10 mA cm^{-2}, with the cost normalized performance greatly surpassing the state-of-the-art catalysts. After a 20 hour stability test at 10 mA cm^{-2}, only 50 mV overpotential increase was noticed. To investigate the practical application potential, a PEM water electrolyzer using the IrRu alloy on TiC as the anode catalyst was assembled, which required a cell voltage of only 1.48 V to reach a current density of 1 A cm^{-2}.

Results and discussion

Structure characterization

The IrRu alloy nanoparticles (NPs) with different Ir/Ru ratios (denoted as Ir_xRu_y) loaded on oxygenated TiC were synthesized through reduction in ethylene glycol. The physical structure of Ir_xRu_y/TiC was characterized by high-resolution transmission electron microscopy (HRTEM), as shown in Fig. 1. An intense signal of TiC was found in the HRTEM image with a lattice spacing of about 0.22 nm corresponding to the (111) facet. The existence of the TiO_2 signal indicates the native oxidation of TiC, which was also reported in previous works.[45] The native oxide could help NPs to be bonded more strongly to the surface of TiC. Ir_xRu_y NPs with diameters of about 3–5 nm can be found uniformly decorated over the oxidized TiC support. Lattice spacings of 0.207 nm and 0.213 nm can be assigned to the (101) and (002) facets of the Ru(hcp) structure, respectively, while the lattice spacing of 0.22 nm corresponds to the (111) facet of the Ir(fcc) structure. The hcp structure was found to dominate in Ir_1Ru_4/TiC, while the fcc structure dominates in Ir_1Ru_1/TiC. A similar structure was also observed in the high-angle annular dark-field (HADDF) imaging, as shown in Fig. S2 and S3.† The X-ray diffraction (XRD) pattern, as displayed in Fig. S1,† shows a weakening of the Ru signal with decreasing Ru content, which corresponds well with other reports on the IrRu alloy.[36]

To examine the geometric and electronic structure of the as-prepared IrRu alloy, X-ray absorption spectroscopy (XAS) was performed. As shown in the X-ray near-edge fine structure (XANES), the white line intensity of Ir in Ir_xRu_y/TiC gradually increases with increasing Ru content (Fig. 1d), corresponding to increasing electron transition from the occupied $2p_{3/2}$ orbital to the partially occupied Ir 5d orbitals. This suggests a similar density of unoccupied Ir 5d orbitals in Ir_xRu_y/TiC with different Ir/Ru ratios. The threshold position for Ru in Ir_xRu_y/TiC shifts positively with increasing Ru content, suggesting an increase in the Ru valence state (Fig. 1g). These results are reasonable as Ir and Ru can be both oxidized in air, and Ru is more easily oxidized as compared to Ir.[3] The Fourier-transformed extended X-ray absorption fine structure (EXAFS) spectra are shown in Fig. 1e and h, with detailed fitting results displayed in Fig. S5 and S6.†

Tables S2 and S3† show that the Ir–Ir intensity decreases while Ru–M intensity increases with decreasing Ir/Ru ratio. The corresponding wavelet transform plots are also presented in Fig. 1f and i, from which the intensity shifts were observed between neighboring Ir- and Ru-centered coordination. Based on IrO_2 and RuO_2 standard sample profiles, the peak with the lowest coordination radius was assigned to M–O (metal–oxide) coordination. With increase *k* and *R*, M–Ir and M–Ru peaks were gradually seen. This again confirms the compositional analysis from the EXAFS and TEM results.

In situ surface enrichment characterization

To investigate how the surface structure of Ir_xRu_y/TiC evolves during OER, *in situ* XAS was conducted. Ir_1Ru_4/TiC was examined because of its high measured stability. With increasing applied anodic potential, the white line intensity of Ir for Ir_1Ru_4/TiC gradually increases, with an average Ir valence state higher than +4 when the potential exceeds 1.5 V *vs.* saturated calomel electrode (SCE) (Fig. 2a and S7a†). The high-valence Ir is recognized as the active site for OER.[18,46] The Fourier transformed EXAFS shows the same trend of iridium oxidation along

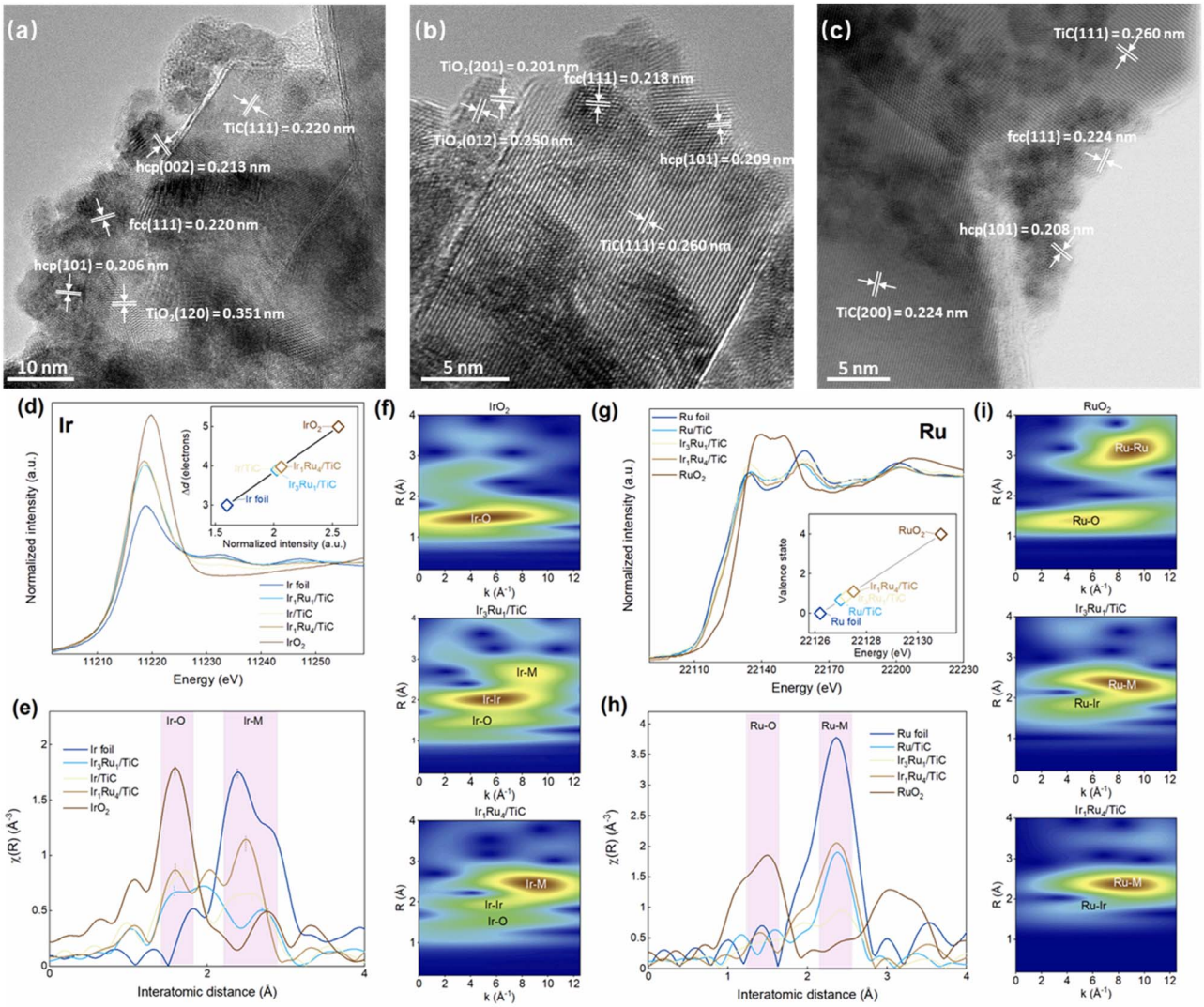

Fig. 1 HRTEM image of (a) Ir_1Ru_4/TiC, (b) Ir_1Ru_1/TiC, and (c) Ir_3Ru_1/TiC. (d) XANES, (e) Fourier transformed EXAFS, and (f) the corresponding wavelet transform of EXAFS for Ir in Ir_xRu_y/TiC. (g) XANES, (h) Fourier transformed EXAFS, and (i) the corresponding wavelet transform of EXAFS for Ru in Ir_xRu_y/TiC. Inset in (d) and (e) show the valence state change.

with applied anodic potential (Fig. 2c). However, the *in situ* XANES spectra of Ru show that the Ru in Ir_1Ru_4/TiC maintains a low valence state (less than +2) with increasing applied anodic potential, even at 1.6 V *vs.* RHE (Fig. 2b and S7b†). This is further confirmed by the *in situ* Fourier transformed EXAFS spectra, which displays constant intensity of Ru–O coordination along with increasing anodic potential (Fig. 2d).

Ir oxidizes drastically, while Ru maintains a low valence state under OER condition, which may seem to be against the conventional understanding that Ru can oxidize more easily than Ir. To explain this unusual observation, we characterized the surface structure change of Ir_1Ru_4/TiC using the electrochemical Cu stripping method (Fig. 2e). After OER, the Ir_1Ru_4/TiC catalyst was first reduced at 0.02 V *vs.* SCE for 300 s and then transferred into another electrolyte with the Cu precursor for the subsequent deposition of Cu. Afterward, the catalyst was transferred into a Cu-free electrolyte to perform cyclic voltammetry measurement. As shown in Fig. 2e, the peak appearing at about 0.3 V *vs.* RHE is associated with bulk Cu deposition, and the peaks at about 0.4 V and 0.55 V *vs.* RHE can be assigned to Cu underpotential deposition (UPD) over Ru and Ir, respectively.[39] It can be found that the surface Ru content rapidly decreased after a few OER cycles. However, the Ir signal can still be found even after 75 CV cycles. This provides a strong proof that the catalyst's surface was *in situ* transformed into an Ir-enriched surface after OER, possibly due to ruthenium oxide dissolution. By quantifying the coordination number from Fourier transformed EXAFS, the trend of change in Ir coordination is displayed in Fig. S8 and Table S4.† The increase in Ir–O coordination confirms that the surface was gradually oxidized with increasing anodic potential. Interestingly, the ratio of Ir–Ru coordination to Ir–Ir coordination also decreases with increasing anodic potential, indicating that the surface was gradually covered with Ir oxide, while the surface Ru was etched into the solution.

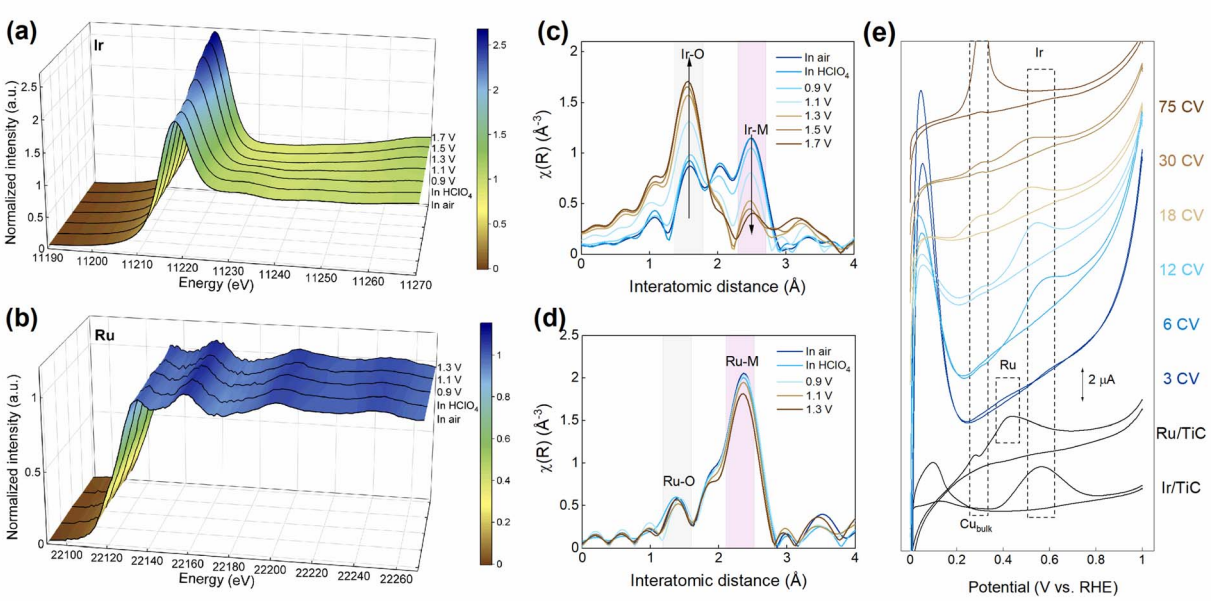

Fig. 2 *In situ* XANES for (a) Ir and (b) Ru. *In situ* Fourier transformed EXAFS for (c) Ir and (d) Ru in Ir_1Ru_4/TiC. (e) Cu stripping of Ir_1Ru_4/TiC.

Theoretical investigation

The *in situ* surface enrichment of Ir on the IrRu alloy during OER was confirmed by advanced spectroscopic and electrochemical characterization. To investigate how this unique Ir-enriched surface structure influences the OER performance of the IrRu alloy, density functional theory (DFT) calculations were performed on Ir_1Ru_3, Ir_1Ru_1, Ir_3Ru_1, and pure Ir, representing the Ir_xRu_y alloy with different Ir/Ru ratios (Fig. 3a). All the surfaces were covered with a thin layer of Ir oxide to simulate the Ir-enriched surface. Due to the higher electronegativity of Ir as compared to Ru, electrons move from Ru to Ir in the bulk IrRu alloy and more negative charges accumulate on Ir along with the decreasing Ir/Ru ratio (Fig. S9†). The charge of the Ir atoms in the Ir oxide layer follows the same trend as that in the bulk (Fig. 3b). The d-band center of the active site near the Fermi level is usually linked with the adsorption energetics of reactive intermediates.[47,48] As shown in Fig. 3b and S10,† the d-band center of the Ir atoms in the Ir oxide layer decreases from Ir_3Ru_1 to Ir_1Ru_3, indicating the weaker adsorption of oxygenated species on the Ir_xRu_y alloy with a lower Ir/Ru ratio.

Then, we calculated the energetics of OER at $T = 298.15$ K and $P = 1$ atm (Fig. 3c). It was found that the rate-determining step (RDS) of OER is at the 3rd electron-transfer step, namely, the oxidation of O* to OOH*, which is limited by the weak adsorption of OOH* on Ir_1Ru_3, Ir_1Ru_1, Ir_3Ru_1, and Ir with a free energy barrier of 0.45 eV, 0.49 eV, 0.51 eV, and 0.52 eV, respectively (Fig. 3c). Thus, we can predict that the OER activity on the Ir_xRu_y alloy will follow an increasing order along with decreasing Ir/Ru ratio. However, with increasing Ru content in the Ir_xRu_y alloy, the surface Ru atoms can be more easily

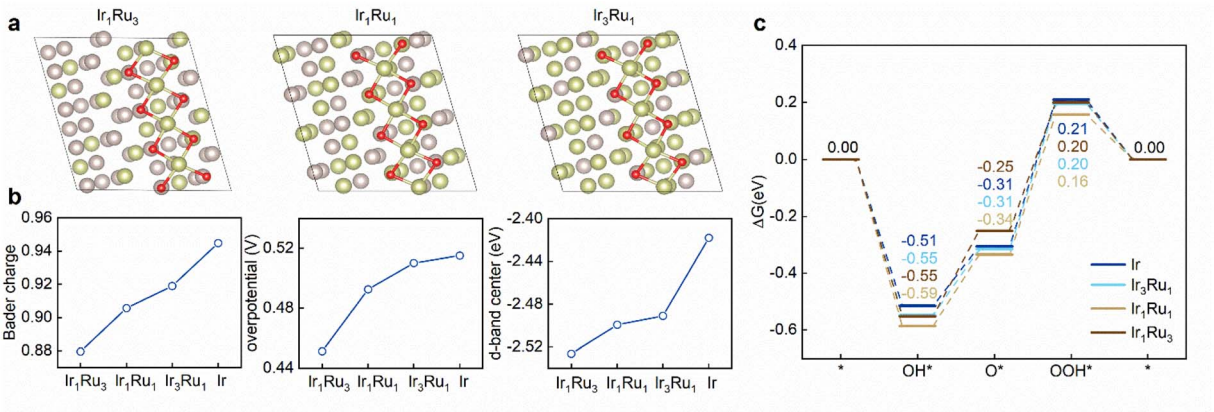

Fig. 3 (a) Structural models of Ir_1Ru_3, Ir_1Ru_1, and Ir_3Ru_1 used in the DFT calculation. The balls in green, brown, and red represent Ir, Ru, and O atoms, respectively. (b) The calculated Bader charge of Ir atom in the Ir oxide layer, overpotential of OER, and d-band center of Ir atom in the Ir oxide layer. (c) Calculated OER Gibbs free energy diagram at 1.23 V *vs.* RHE, $T = 298.15$ K, and $P = 1$ atm.

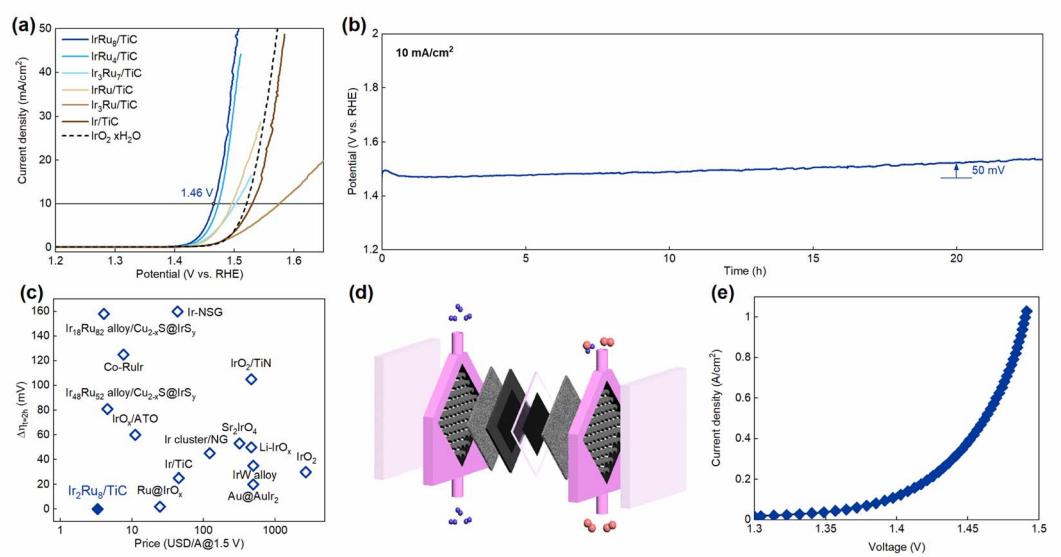

Fig. 4 (a) Polarization curves. (b) Stability of Ir_1Ru_4/TiC measured at 10 mA cm^{-2}. (c) Comparison of cost per ampere @ 1.5 V (*vs.* RHE) and overpotential change before and after 2 hours of reaction. (d) Schematic plot displaying the assembly of the PEM water electrolyzer. Purple and pink balls represent hydrogen and oxygen atoms. (e) Polarization curve of the PEM water electrolyzer (anode catalyst loading: 0.3 mg_{Ir} cm^{-2}).

leached, causing an instability issue. Therefore, tuning the ratio of Ir/Ru in the Ir_xRu_y alloy to balance the OER activity and stability is crucial to deliver optimal catalytic performance.

Electrocatalytic performance

The electrocatalytic performance of the Ir_xRu_y alloy NPs with different Ir/Ru ratios was examined in 0.1 M $HClO_4$ solution. As shown in Fig. 4a, the linear sweep voltammetry (LSV) test indicates the highest OER activity for Ir_1Ru_4/TiC, which exhibits the lowest overpotential of only 230 mV at 10 mA cm^{-2}, surpassing the commercial IrO_2 catalyst and most state-of-the-art OER catalysts reported in the literature. The OER performance of other Ir_xRu_y/TiC is displayed in Fig. 4a with the activity trend matching well with the DFT prediction. Besides the activity, the stability of the catalyst was examined by chronopotentiometry at 10 mA cm^{-2}, as displayed in Fig. 4b. The Ir_1Ru_4/TiC can be sustained for more than 20 hours with less than 50 mV potential increase, which also surpasses most of the noble-metal-based OER catalysts in acid reported in the literature (Table S7†). From the inductively coupled plasma-optical emission spectrometry (ICP-OES) results of the samples before and after the 5 hour OER test (Table S1†), the Ir/Ru ratio could be quantified to change from 1 : 3.9 to 1 : 2.5, corresponding to the fast dissolution of Ru and surface enrichment of Ir, as shown before. Apart from the activity and stability, economic consideration is also crucial for the large-scale deployment of the PEM water electrolyzer. We compared the activity normalized by the noble metal cost, as shown in Fig. 4c, together with the stability (detailed comparison can be found in Table S7†). It is clear that Ir_1Ru_4/TiC outperforms the other acidic OER catalysts, reaching a current of 1 A at the cost of 3.3 USD. To further study the practical application potential at an industrialized scale, a PEM water electrolyzer was assembled using the as-prepared Ir_1Ru_4/TiC as the anode catalyst (Fig. 4d), which is able to deliver a current density of 1 A cm^{-2} at a cell voltage as low as 1.49 V.

Conclusion

OER-induced surface enrichment of Ir on the IrRu alloy targeted for excellent OER performance was for the first time probed by *ex situ* high-resolution transmission electron microscopy, *in situ* X-ray absorption spectroscopy, and electrochemical Cu stripping. The characterization results indicated the fast dissolution of Ru and oxidation to form an active and protective Ir oxide shell on the surface of the IrRu alloy during OER. The Ir-enriched surface not only protected Ru in the core against oxidation but also offered catalytically active sites that drive the water oxidation reaction. Furthermore, the core with a high content of Ru could not only optimize the electronic structure of the Ir shell, but also significantly reduce the Ir usage, which allowed the Ir_1Ru_4/TiC catalyst to deliver a current of 1 A at a cost of only 3.3 USD, significantly outperforming the other acidic OER catalysts reported in the literature.

Data availability

All data is available in the main text or the ESI.†

Author contributions

J. Z., X. L. and L. B. designed the idea. J. Z. and X. L. conducted the material synthesis and characterizations. Y.-F. J. and C. Q. X., and J. L. conducted the density functional theory calculation. S.-F. H. conducted the in-situ XAS characterization. W. L.

conducted the high resolution TEM characterization. J. Z., X. C., H. B. Y., D-S. L., T. Z., Y. L., J. L., and B. L. write the manuscript.

Conflicts of interest

Authors declare no competing interests.

Acknowledgements

This work was supported by the funds from the Singapore Ministry of Education Academic Research Fund (AcRF) Tier 1: RG4/20, RG2/21, and Tier 2: MOET2EP10120-0002. J.L. and C.-Q.X. acknowledge financial support from the National Natural Science Foundation of China (22033005 and 22103035) and Guangdong Basic and Applied Basic Research Foundation (2020A1515110282). This work was partially sponsored by the Guangdong Provincial Key Laboratory of Catalysis (No. 2020B121201002). Computational resources were supported by Taizi high-performance supercomputer cluster of Center for Computational Science and Engineering of Southern University of Science and Technology, and high-performance supercomputer cluster of Department of Chemistry (CHEM-HPC) of Southern University of Science and Technology.

References

1 Q. Shi, C. Zhu, D. Du and Y. Lin, Robust noble metal-based electrocatalysts for oxygen evolution reaction, *Chem. Soc. Rev.*, 2019, **48**, 3181–3192.

2 T. Reier, Z. Pawolek, S. Cherevko, M. Bruns, T. Jones, D. Teschner, S. Selve, A. Bergmann, H. N. Nong, R. Schlogl, *et al.*, Molecular insight in structure and activity of highly efficient, low-Ir Ir-Ni oxide catalysts for electrochemical water splitting (OER), *J. Am. Chem. Soc.*, 2015, **137**, 13031–13040.

3 K. Klyukin, A. Zagalskaya and V. Alexandrov, Role of dissolution intermediates in promoting oxygen evolution reaction at RuO_2(110) Surface, *J. Phys. Chem. C*, 2019, **123**, 22151–22157.

4 Z. L. Zhao, Q. Wang, X. Huang, Q. Feng, S. Gu, Z. Zhang, H. Xu, L. Zeng, M. Gu and H. Li, Boosting the oxygen evolution reaction using defect-rich ultra-thin ruthenium oxide nanosheets in acidic media, *Energy Environ. Sci.*, 2020, 5143–5151.

5 Y. Lin, Z. Tian, L. Zhang, J. Ma, Z. Jiang, B. J. Deibert, R. Ge and L. Chen, Chromium-ruthenium oxide solid solution electrocatalyst for highly efficient oxygen evolution reaction in acidic media, *Nat. Commun.*, 2019, **10**, 162.

6 J. Shan, T. Ling, K. Davey, Y. Zheng and S. Z. Qiao, Transition-metal-doped ruir bifunctional nanocrystals for overall water splitting in acidic environments, *Adv. Mater.*, 2019, **31**, e1900510.

7 O. Kasian, J. P. Grote, S. Geiger, S. Cherevko and K. J. J. Mayrhofer, The common intermediates of oxygen evolution and dissolution reactions during water electrolysis on iridium, *Angew. Chem., Int. Ed. Engl.*, 2018, **57**, 2488–2491.

8 Y. Yao, S. Hu, W. Chen, Z.-Q. Huang, W. Wei, T. Yao, R. Liu, K. Zang, X. Wang, G. Wu, *et al.*, Engineering the electronic structure of single atom Ru sites *via* compressive strain boosts acidic water oxidation electrocatalysis, *Nat. Catal.*, 2019, **2**, 304–313.

9 Q. Wang, C. Q. Xu, W. Liu, S. F. Hung, H. Bin Yang, J. Gao, W. Cai, H. M. Chen, J. Li and B. Liu, Coordination engineering of iridium nanocluster bifunctional electrocatalyst for highly efficient and pH-universal overall water splitting, *Nat. Commun.*, 2020, **11**, 4246.

10 X. Wu, B. Feng, W. Li, Y. Niu, Y. Yu, S. Lu, C. Zhong, P. Liu, Z. Tian, L. Chen, *et al.*, Metal-support interaction boosted electrocatalysis of ultrasmall iridium nanoparticles supported on nitrogen doped graphene for highly efficient water electrolysis in acidic and alkaline media, *Nano Energy*, 2019, **62**, 117–126.

11 G. Li, K. Li, L. Yang, J. Chang, R. Ma, Z. Wu, J. Ge, C. Liu and W. Xing, Boosted performance of Ir species by employing tin as the support toward oxygen evolution reaction, *ACS Appl. Mater. Interfaces*, 2018, **10**, 38117–38124.

12 K. Zhang, W. Mai, J. Li, H. Wang, G. Li and W. Hu, Highly scattered Ir oxides on TiN as an efficient oxygen evolution reaction electrocatalyst in acidic media, *J. Mater. Sci.*, 2019, **55**, 3507–3520.

13 J. Joo, H. Jin, A. Oh, B. Kim, J. Lee, H. Baik, S. H. Joo and K. Lee, An IrRu alloy nanocactus on $Cu_{2-x}S$@IrS_y as a highly efficient bifunctional electrocatalyst toward overall water splitting in acidic electrolytes, *J. Mater. Chem. A*, 2018, **6**, 16130–16138.

14 H. S. Oh, H. N. Nong, T. Reier, A. Bergmann, M. Gliech, J. Ferreira de Araujo, E. Willinger, R. Schlogl, D. Teschner and P. Strasser, Electrochemical catalyst-support effects and their stabilizing role for irox nanoparticle catalysts during the oxygen evolution reaction, *J. Am. Chem. Soc.*, 2016, **138**, 12552–12563.

15 P. Kúš, A. Ostroverkh, K. Ševčíková, I. Khalakhan, R. Fiala, T. Skála, N. Tsud and V. Matolin, Magnetron sputtered Ir thin film on TiC-based support sublayer as low-loading anode catalyst for proton exchange membrane water electrolysis, *Int. J. Hydrogen Energy*, 2016, **41**, 15124–15132.

16 R. E. Fuentes, H. R. Colón-Mercado and M. J. Martínez-Rodríguez, PT-Ir/TiC electrocatalysts for PEM fuel cell/electrolyzer process, *J. Electrochem. Soc.*, 2013, **161**, F77–F82.

17 H. Wang, Z. N. Chen, D. Wu, M. Cao, F. Sun, H. Zhang, H. You, W. Zhuang and R. Cao, Significantly Enhanced Overall Water Splitting Performance by Partial Oxidation of Ir through Au Modification in Core-Shell Alloy Structure, *J. Am. Chem. Soc.*, 2021, **143**, 4639–4645.

18 J. Gao, X. Huang, W. Cai, Q. Wang, C. Jia and B. Liu, Rational design of an iridium-tungsten composite with an iridium-rich surface for acidic water oxidation, *ACS Appl. Mater. Interfaces*, 2020, **12**, 25991–26001.

19 A. L. Strickler, D. Higgins and T. F. Jaramillo, Crystalline strontium iridate particle catalysts for enhanced oxygen evolution in acid, *ACS Appl. Energy Mater.*, 2019, **2**, 5490–5498.

20 L. C. Seitz, C. F. Dickens, K. Nishio, Y. Hikita, J. Montoya, A. Doyle, C. Kirk, A. Vojvodic, H. Y. Hwang, J. K. Norskov, *et al.*, A highly active and stable IrOx/$SrIrO_3$ catalyst for the oxygen evolution reaction, *Science*, 2016, **353**, 1011–1014.

21 J. Gao, C. Q. Xu, S. F. Hung, W. Liu, W. Cai, Z. Zeng, C. Jia, H. M. Chen, H. Xiao, J. Li, *et al.*, Breaking long-range order in iridium oxide by alkali ion for efficient water oxidation, *J. Am. Chem. Soc.*, 2019, **141**, 3014–3023.

22 S.-A. Park, K. Shim, K.-S. Kim, Y. H. Moon and Y.-T. Kim, Enhanced activity for oxygen evolution reaction of nanoporous irni thin film formed by electrochemical selective etching process, *J. Electrochem. Sci. Technol.*, 2019, **10**, 402–407.

23 H. N. Nong, T. Reier, H.-S. Oh, M. Gliech, P. Paciok, T. H. T. Vu, D. Teschner, M. Heggen, V. Petkov, R. Schlögl, *et al.*, A unique oxygen ligand environment facilitates water oxidation in hole-doped IrNiOx core–shell electrocatalysts, *Nat. Catal.*, 2018, **1**, 841–851.

24 S. Xu, S. Chen, L. Tian, Q. Xia and W. Hu, Selective-leaching method to fabricate an Ir surface-enriched Ir-Ni oxide electrocatalyst for water oxidation, *J. Solid State Electrochem.*, 2016, **20**, 1961–1970.

25 J. Kim, P. C. Shih, Y. Qin, Z. Al-Bardan, C. J. Sun and H. Yang, A porous pyrochlore $Y_2[Ru_{1.6}Y_{0.4}]O_{7-\delta}$ electrocatalyst for enhanced performance towards the oxygen evolution reaction in acidic media, *Angew. Chem., Int. Ed. Engl.*, 2018, **57**, 13877–13881.

26 S. W. Lee, B. H. Lee, T.-Y. Kim, C. Baik, M. S. Kim, G. S. Chai and C. Pak, Multifunctional non-Pt ternary catalyst for the hydrogen oxidation and oxygen evolution reactions in reversal-tolerant anode, *Catal. Commun.*, 2019, **130**, 105758.

27 F. Ye, C. Xu, G. Liu, J. Li, X. Wang, X. Du and J. K. Lee, A novel PtRuIr nanoclusters synthesized by selectively electrodepositing Ir on PtRu as highly active bifunctional electrocatalysts for oxygen evolution and reduction, *Energy Convers. Manage.*, 2018, **155**, 182–187.

28 A. R. Zeradjanin, N. Menzel, W. Schuhmann and P. Strasser, On the faradaic selectivity and the role of surface inhomogeneity during the chlorine evolution reaction on ternary Ti-Ru-Ir mixed metal oxide electrocatalysts, *Phys. Chem. Chem. Phys.*, 2014, **16**, 13741–13747.

29 M. Min, E. You, S. W. Lee and C. Pak, Cathode durability enhancement under start-up/shut-down process using IrRuOx/C catalyst in polymer electrolyte membrane fuel cell, *J. Power Sources*, 2021, **488**, 229423.

30 J. R. De Lile, A. Bahadoran, Q. Liu, S. Woo Lee, C. Pak, J. Zhang and S. G. Lee, First principles study of Ir_3Ru, IrRu and $IrRu_3$ catalysts for hydrogen oxidation reaction: Effect of surface modification and ruthenium content, *Appl. Surf. Sci.*, 2021, **545**, 149002.

31 T.-Y. Kim, S. W. Lee and C. Pak, Optimization of carbon-supported Ir–Ru alloys for polymer electrolyte fuel cell anodes under cell reversal, *J. Ind. Eng. Chem.*, 2020, **85**, 87–93.

32 Y. Inami, S. Iguchi, S. Nagamatsu, K. Asakura and I. Yamanaka, Disposition of iridium on ruthenium nanoparticle supported on ketjenblack: Enhancement in electrocatalytic activity toward the electrohydrogenation of toluene to methylcyclohexane, *ACS Omega*, 2020, **5**, 1221–1228.

33 J. Shan, C. Guo, Y. Zhu, S. Chen, L. Song, M. Jaroniec, Y. Zheng and S.-Z. Qiao, Charge-redistribution-enhanced nanocrystalline Ru@IrOx electrocatalysts for oxygen evolution in acidic media, *Chem*, 2019, **5**, 445–459.

34 E. You, M. Min, S.-A. Jin, T. Kim and C. Pak, Highly durable, cost-effective, and multifunctional carbon-supported IrRu-based catalyst for automotive polymer electrolyte fuel cell anodes, *J. Electrochem. Soc.*, 2018, **165**, F3094–F3099.

35 M. Faustini, M. Giraud, D. Jones, J. Rozière, M. Dupont, T. R. Porter, S. Nowak, M. Bahri, O. Ersen, C. Sanchez, *et al.*, Hierarchically structured ultraporous iridium-based materials: A novel catalyst architecture for proton exchange membrane water electrolyzers, *Adv. Energy Mater.*, 2019, **9**, 1802136.

36 Y. Inami, H. Ogihara, S. Nagamatsu, K. Asakura and I. Yamanaka, Synergy of Ru and Ir in the electrohydrogenation of toluene to methylcyclohexane on a ketjenblack-supported Ru-Ir alloy cathode, *ACS Catal.*, 2019, **9**, 2448–2457.

37 Z. Ma, Y. Zhang, S. Liu, W. Xu, L. Wu, Y.-C. Hsieh, P. Liu, Y. Zhu, K. Sasaki, J. N. Renner, *et al.*, Reaction mechanism for oxygen evolution on RuO_2, IrO_2, and RuO_2@IrO_2 core-shell nanocatalysts, *J. Electroanal. Chem.*, 2018, **819**, 296–305.

38 L. Wang, V. A. Saveleva, S. Zafeiratos, E. R. Savinova, P. Lettenmeier, P. Gazdzicki, A. S. Gago and K. A. Friedrich, Highly active anode electrocatalysts derived from electrochemical leaching of Ru from metallic $Ir_{0.7}Ru_{0.3}$ for proton exchange membrane electrolyzers, *Nano Energy*, 2017, **34**, 385–391.

39 J. Ohyama, D. Kumada and A. Satsuma, Improved hydrogen oxidation reaction under alkaline conditions by ruthenium–iridium alloyed nanoparticles, *J. Mater. Chem. A*, 2016, **4**, 15980–15985.

40 T. Audichon, T. W. Napporn, C. Canaff, C. Morais, C. Comminges and K. B. Kokoh, IrO_2 coated on RuO_2 as efficient and stable electroactive nanocatalysts for electrochemical water splitting, *J. Phys. Chem. C*, 2016, **120**, 2562–2573.

41 K. Sardar, E. Petrucco, C. I. Hiley, J. D. Sharman, P. P. Wells, A. E. Russell, R. J. Kashtiban, J. Sloan and R. I. Walton, Water-splitting electrocatalysis in acid conditions using ruthenate-iridate pyrochlores, *Angew. Chem., Int. Ed. Engl.*, 2014, **53**, 10960–10964.

42 N. Danilovic, R. Subbaraman, K. C. Chang, S. H. Chang, Y. Kang, J. Snyder, A. P. Paulikas, D. Strmcnik, Y. T. Kim, D. Myers, *et al.*, Using surface segregation to design stable Ru-Ir oxides for the oxygen evolution reaction in acidic environments, *Angew. Chem., Int. Ed. Engl.*, 2014, **53**, 14016–14021.

43 L.-E. Owe, M. Tsypkin, K. S. Wallwork, R. G. Haverkamp and S. Sunde, Iridium–ruthenium single phase mixed oxides for oxygen evolution: Composition dependence of electrocatalytic activity, *Electrochim. Acta*, 2012, **70**, 158–164.

44 H. N. Nong, L. Gan, E. Willinger, D. Teschner and P. Strasser, IrOx core-shell nanocatalysts for cost- and energy-efficient electrochemical water splitting, *Chem. Sci.*, 2014, **5**, 2955–2963.

45 J. Zhang, J. Ma, T. S. Choksi, D. Zhou, S. Han, Y. F. Liao, H. B. Yang, D. Liu, Z. Zeng, W. Liu, *et al.*, Strong metal-support interaction boosts activity, selectivity, and stability in electrosynthesis of H_2O_2, *J. Am. Chem. Soc.*, 2022, **144**, 2255–2263.

46 H. Ooka, Y. Wang, A. Yamaguchi, M. Hatakeyama, S. Nakamura, K. Hashimoto and R. Nakamura, Legitimate intermediates of oxygen evolution on iridium oxide revealed by *in situ* electrochemical evanescent wave spectroscopy, *Phys. Chem. Chem. Phys.*, 2016, **18**, 15199–151204.

47 J. Zhang, H. B. Tao, M. Kuang, H. B. Yang, W. Cai, Q. Yan, Q. Mao and B. Liu, Advances in thermodynamic-kinetic model for analyzing the oxygen evolution reaction, *ACS Catal.*, 2020, **10**, 8597–8610.

48 J. Zhang, W. Xu, Y. Liu, S.-F. Hung, W. Liu, Z. Lam, H. B. Tao, H. Yang, W. Cai, H. Xiao, *et al.*, *In situ* precise tuning of bimetallic electronic effect for boosting oxygen reduction catalysis, *Nano Lett.*, 2021, **21**, 7753–7760.